The EMBO Journal (2007) 26, 2454–2464 | © 2007 European Molecular Biology Organization | All Rights Reserved 0261-4189/07
www.embojournal.org

THE EMBO JOURNAL

Dual mechanisms specify Doa4-mediated deubiquitination at multivesicular bodies

Caleb Richter, Matthew West and Greg Odorizzi*

Department of Molecular, Cellular, and Developmental Biology, University of Colorado, Boulder, CO, USA

Doa4 is a ubiquitin-specific protease in *Saccharomyces cerevisiae* that deubiquitinates integral membrane proteins sorted into the lumenal vesicles of late-endosomal multivesicular bodies (MVBs). We show that the non-catalytic N terminus of Doa4 mediates its recruitment to endosomes through its association with Bro1, which is one of several highly conserved class E Vps proteins that comprise the core MVB sorting machinery. In turn, Bro1 directly stimulates deubiquitination by interacting with a YPxL motif in the catalytic domain of Doa4. Mutations in either Doa4 or Bro1 that disrupt catalytic activation of Doa4 impair deubiquitination and sorting of MVB cargo proteins and lead to the formation of lumenal MVB vesicles that are predominantly small compared with the vesicles seen in wild-type cells. Thus, by recruiting Doa4 to late endosomes and stimulating its catalytic activity, Bro1 fulfills a novel dual role in coordinating deubiquitination in the MVB pathway.

The EMBO Journal (2007) **26,** 2454–2464. doi:10.1038/sj.emboj.7601692; Published online 19 April 2007
Subject Categories: membranes & transport
Keywords: deubiquitination; endosomes; multivesicular bodies; protein sorting

Introduction

Deubiquitinating enzymes (DUBs) catalyze removal of ubiquitin (Ub) from proteins targeted for degradation, thereby replenishing the pool of free cellular Ub. DUBs also function in non-proteolytic processes such as cleavage of inactive poly-Ub translational fusions and deubiquitination of histones, which regulate chromosome condensation and transcriptional silencing during mitosis (Kim *et al*, 2003; Amerik and Hochstrasser, 2004). The Ub-specific protease (UBP) family encompasses the majority of DUBs identified by sequence homology (Clague and Urbe, 2006). Many UBPs are coupled to specific cellular processes, but the factors that determine their functional specificities are largely uncharacterized.

Doa4 is a UBP in *Saccharomyces cerevisiae* that functions in the multivesicular body (MVB) protein sorting pathway, where it deubiquitinates integral membrane proteins ubiquitinated on their cytosolic domains. Monoubiquitination (or, in some cases, polyubiquitination with a short chain of 2–3 Ub subunits) targets membrane proteins into lumenal MVB vesicles formed by invagination of the late-endosomal membrane (Dupre and Haguenauer-Tsapis, 2001; Katzmann *et al*, 2001; Reggiori and Pelham, 2001; Urbanowski and Piper, 2001). Lumenal MVB vesicles and their cargoes are ultimately delivered into the hydrolytic interior of the vacuole upon fusion of the limiting endosomal membrane with the vacuolar membrane. Doa4 ensures that Ub is recovered from cargoes before their enclosure within lumenal vesicles (Dupre and Haguenauer-Tsapis, 2001; Katzmann *et al*, 2001; Losko *et al*, 2001). Recruitment of Doa4 to late endosomes involves Bro1, one of several highly conserved 'class E' Vps proteins that comprise the core machinery required for MVB cargo sorting and lumenal vesicle formation (Luhtala and Odorizzi, 2004). Bro1-mediated recruitment of Doa4 occurs downstream of cargo recognition, which is executed by Ub-binding class E Vps proteins of the endosomal sorting complexes required for transport (ESCRTs) (Hurley and Emr, 2006).

In mammalian cells, ubiquitinated membrane proteins are similarly recognized by orthologs of the class E Vps machinery and deubiquitinated by UBPY, the mammalian ortholog of Doa4 (Mizuno *et al*, 2005; Row *et al*, 2006). Mammalian class E Vps proteins are also commandeered by many enveloped viruses to facilitate budding of infectious virions from host cells, which is a Ub-dependent process topologically equivalent to the budding of lumenal MVB vesicles (Morita and Sundquist, 2004). Class E Vps proteins are recruited to the site of viral budding through interaction with 'late domain' motifs in virally encoded proteins. Alix, the mammalian ortholog of Bro1, binds the YPxL late domain motif in the Gag subunit of human immunodeficiency virus-1 (HIV-1), equine infectious anemia virus (EIAV), and murine leukemia virus (MuLV) (Martin-Serrano *et al*, 2003; Strack *et al*, 2003; Segura-Morales *et al*, 2005). Transplantation of YPxL into a recombinant retrovirus results in enhanced deubiquitination of Gag (Martin-Serrano *et al*, 2004), suggesting that Alix mediates recruitment of UBPY (or a different DUB) in a manner analogous to recruitment of Doa4 by Bro1.

In addition to its role in the MVB pathway, Doa4 functions in removal of poly-Ub from soluble proteins targeted for degradation at proteasomes (Papa *et al*, 1999) and is implicated in the control of DNA replication and repair (Singer *et al*, 1996; Fiorani *et al*, 2004). Regulating Doa4 specificity in multiple cellular processes is likely to be dependent upon mechanisms that control its subcellular localization. However, we report that, alone, localization of Doa4 to endosomes is insufficient for specifying deubiquitination of MVB cargo proteins. Doa4 must also be activated upon its recruitment to endosomal membranes. Bro1 fulfills both roles by associating with the non-catalytic N-terminal region of Doa4 to mediate its localization to endosomes and by

*Corresponding author. Department of Molecular, Cellular, and Developmental Biology, University of Colorado, 347 UCB, Colorado Avenue, Boulder, CO 80309, USA. Tel.: +1 303 735 0179; Fax: +1 303 492 7744; E-mail: odorizzi@colorado.edu

Received: 29 November 2006; accepted: 29 March 2007; published online: 19 April 2007

interacting with the catalytic domain of Doa4 to stimulate deubiquitination. Enzymatic activation of Doa4 occurs through binding of a conserved proline-based sequence located near the C terminus of Bro1 to a YPxL motif in Doa4. Mutations that prevent Bro1 from activating Doa4 disrupt deubiquitination and sorting of MVB cargo proteins. Thus, Bro1 coordinates Doa4 function and specificity by recruiting Doa4 to the MVB and acting as a cofactor to enhance deubiquitination.

Results

Bro1 associates with the N-terminal region of Doa4 to mediate its recruitment to endosomes

Doa4 is one of 16 UBPs in *S. cerevisiae*, all of which contain highly conserved C-terminal catalytic domains coupled to N-terminal regions with low similarity among one another (Amerik and Hochstrasser, 2004). The N-terminal regions of UBPs are thought to determine substrate specificity, potentially by mediating localization of each UBP to a distinct subcellular site of function (Kim *et al*, 2003). Indeed, GFP fused to amino acids 1–560 of Doa4 (Doa4^{N}-GFP; Figure 1A) localized to FM4-64-stained endosomes as efficiently as did GFP fused to full-length Doa4 (Doa4-GFP; Figure 1B). Both Doa4^{N}-GFP and Doa4-GFP were observed in cells in which the *VPS4* gene had been deleted (*vps4*Δ). *VPS4* encodes an ATPase that catalyzes dissociation of Doa4 (and class E Vps proteins) from endosomal membranes. Thus, the absence of Vps4 facilitates identification of Doa4 recruitment by trapping it at endosomes (Luhtala and Odorizzi, 2004).

Unlike Doa4^{N}-GFP and Doa4-GFP, GFP was predominantly cytosolic in *vps4*Δ cells when fused to amino acids 561–926 of Doa4, which comprise its catalytic domain (Doa4^{CAT}-GFP; Figure 1C). The N terminus of Doa4, therefore, is both necessary and sufficient for endosomal recruitment. As in the case of full-length Doa4 (Luhtala and Odorizzi, 2004), localization of Doa4^{N}-GFP to endosomes was dependent upon Bro1 (Figure 1D), and this region co-immunoprecipitated with Bro1 from yeast cell lysates (Figure 1E).

The catalytic domain of Doa4 is specifically required for cargo deubiquitination and sorting

To determine whether endosomal localization is sufficient to confer substrate specificity, we tested if the catalytic domain of a different UBP was functional in the MVB pathway when fused to the Doa4 N terminus. Ubp5 is the UBP in yeast most closely related to Doa4 (Figure 2A), but GFP fused to full-length Ubp5 (Ubp5-GFP) failed to localize to endosomes (Figure 2B), consistent with Ubp5 having no functional role in MVB sorting. As expected, appending the Doa4 N-terminal region to the Ubp5 catalytic domain led to endosomal localization of the resulting fusion protein (Doa4^{N}-Ubp5^{CAT}-GFP; Figure 2C). However, GFP-tagged carboxypeptidase S (GFP-CPS), a cargo protein normally sorted into the vacuole lumen via the MVB pathway (Odorizzi *et al*, 1998), was missorted to the vacuole membrane in cells expressing Doa4^{N}-Ubp5^{CAT} in place of wild-type Doa4, similar to the mislocalization of GFP-CPS in *doa4*^{C571S} cells (Figure 2D), which express a catalytically inactive Doa4 mutant. In addition, the Doa4^{N}-Ubp5^{CAT} chimera was unable to deubiquitinate CPS *in vivo* (Figure 2E). Altogether, these observations indicate that the Ubp5 catalytic domain cannot substitute for Doa4 enzymatic activity despite being recruited to the site of Doa4 function at endosomal membranes.

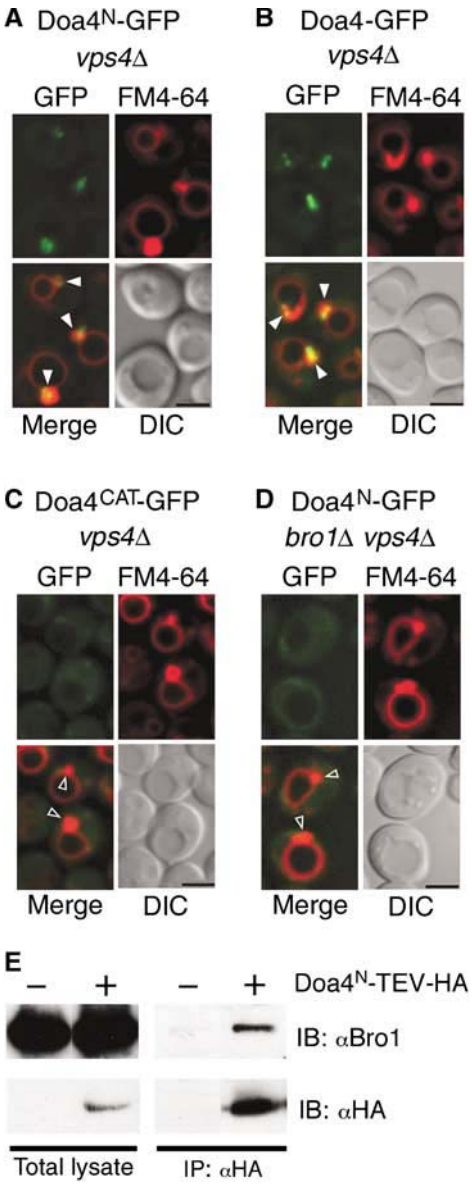

Figure 1 The N terminus of Doa4 is necessary and sufficient for Bro1-mediated localization to endosomes. (**A–D**) Fluorescence and DIC microscopy of Doa4^{N}-GFP, Doa4-GFP, and Doa4^{CAT}-GFP. FM4-64 is a lipophilic stain that specifically labels E compartments and vacuolar membranes. Arrowheads indicate class E compartments that do (closed arrowheads) or do not (open arrowheads) colocalize with GFP. Scale bar, 2.5 μm. (**E**) Native anti-HA immunoprecipitation followed by anti-HA or anti-Bro1 immunoblotting of total lysate versus bound proteins. The GFP fusions in (A–D) and the HA fusion in (E) were expressed from single copies integrated into the genome under the control of the endogenous *DOA4* promoter.

A YPxL motif in the catalytic domain of Doa4 mediates binding to Bro1

The specific requirement for the Doa4 catalytic domain in the MVB pathway led us to compare its amino-acid sequence with that of the Ubp5 catalytic domain. Although the two sequences are ~60% identical, Doa4 contains a YPFL sequence (amino acids 826–829) versus YPYS at the corresponding position in Ubp5 (Figure 2A). The YPFL in Doa4

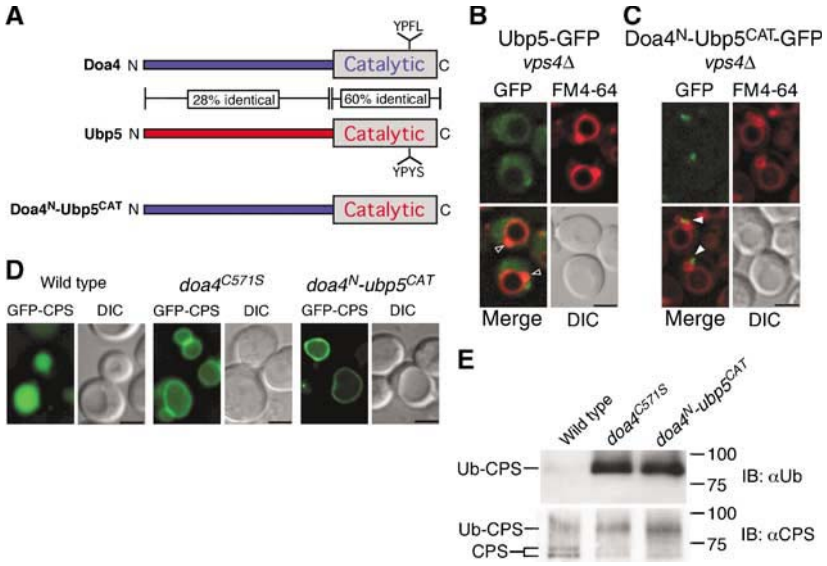

Figure 2 MVB cargo sorting and deubiquitination specifically require the Doa4 catalytic domain. (**A**) Schematic representations of Doa4, Ubp5, and the Doa4^{N}-Ubp5^{CAT} chimera. Amino-acid identity between Doa4 and Ubp5 is indicated. Fluorescence and DIC microscopy of Ubp5-GFP (**B**) or Doa4^{N}-Ubp5^{CAT}-GFP (**C**). Arrowheads indicate class E compartments that do (closed arrowheads) or do not (open arrowheads) colocalize with GFP. (**D**) Fluorescence and DIC microscopy of GFP-CPS. Scale bar, 2.5 μm (B–D). (**E**) Denatured anti-CPS immunoprecipitations followed by anti-Ub or anti-CPS immunoblotting. Doublet bands represent differentially glycosylated forms of CPS. The GFP fusions in (B, C) were expressed from single copies integrated into the genome under the control of the endogenous *DOA4* promoter.

matches the consensus sequence in viral proteins, YPxL, which binds Alix, the mammalian ortholog of Bro1 (Martin-Serrano *et al*, 2003; Strack *et al*, 2003; Segura-Morales *et al*, 2005). Indeed, the YPFL sequence was required for Doa4 function in the MVB pathway. When this motif was changed to AAFA by site-directed mutagenesis (*doa4^{AAFA}*), deubiquitination of CPS was defective (Figure 3B), and GFP-CPS was mislocalized to the vacuole membrane (Figure 3A). Pulse–chase metabolic labeling followed by anti-GFP immunoprecipitation confirmed that the cleavage of GFP from CPS, which occurs following delivery of MVB vesicles into the vacuole lumen and accurately reflects the proteolytic maturation of native CPS (Odorizzi *et al*, 1998), was quantitatively reduced to a similar extent in *doa4^{C571S}* and *doa4^{AAFA}* cells compared with cleavage of GFP-CPS in wild-type cells (Figure 3C). The extent of cleavage was not significantly different in *doa4^{C571S}* and *doa4^{AAFA}* cells expressing lower levels of GFP-CPS (Supplementary Figure S2), nor was the defect in cleavage rescued upon increased Ub expression (Supplementary Figure S3), which agrees with recent work showing that the depleted pools of free Ub, characteristic of *doa4* mutant cells, do not account for MVB sorting defects in cells lacking Doa4 function (Nikko and Andre, 2007). However, GFP-CPS cleavage in *doa4^{C571S}* and *doa4^{AAFA}* cells was not completely blocked, as was observed in *pep4*Δ *prb1*Δ cells lacking vacuolar protease activity (Figure 3C). Thus, the efficiency of GFP-CPS sorting is reduced in the absence of Doa4 function but not completely defective, as seen previously in cells lacking the components of the core MVB sorting machinery of class E Vps proteins, including Vps4 (*vps4*Δ; Figure 3C) (Reggiori and Pelham, 2001; Babst *et al*, 2002). The YPFL motif was not required for recruitment of Doa4 to endosomes (Figure 3D), indicating that, like the Doa4^{N}-Ubp5^{CAT} chimera (Figure 2), Doa4^{AAFA} is unable to function in the MVB pathway despite being recruited to the site of Doa4 activity on endosomal membranes.

Alix binds directly to the YPxL consensus sequence in Gag protein subunits of HIV-1, EIAV, and MuLV (Martin-Serrano *et al*, 2003; Strack *et al*, 2003; Segura-Morales *et al*, 2005). Therefore, we used a yeast two-hybrid assay to test whether Bro1 binds the YPFL motif in Doa4. As a positive control, we used Snf7, which binds directly to the 'Bro1 domain' of Bro1 (Figure 4A) (Kim *et al*, 2005). Accordingly, Snf7 interacted with both full-length Bro1 and the Bro1 domain (amino acids 2–387) but not with the remaining C-terminal fragment of Bro1 (amino acids 388–844; Figure 4B). The catalytic domain of Doa4 also bound full-length Bro1 but did not interact with the Bro1 domain. Instead, the Doa4 catalytic domain bound Bro1$^{388–844}$ (Figure 4B). Because the Doa4 N terminus was removed to preclude the possibility of Bro1 binding it in the two-hybrid assay, Bro1 interacts with the Doa4 catalytic domain independent of the endosomal localization region of Doa4. Binding of Bro1$^{388–844}$ to the Doa4 catalytic domain was abolished, however, when the YPFL motif in Doa4 was changed to AAFL (Figure 4B). Moreover, the Doa4 YPFL motif conforms to the YPxL consensus sequence because individual mutation of Y_{826}, P_{827}, or L_{829}, but not F_{828}, disrupted the interaction with Bro1$^{388–844}$ (Figure 4C). In addition, V_{824} and L_{830} in Doa4 are required for this interaction, whereas I_{825} is dispensable.

Truncation of Bro1 disables it from binding the Doa4 catalytic domain and results in Doa4-specific MVB pathway defects

To map the YPxL-interacting region, we screened a collection of mutant *bro1* alleles for their ability to phenocopy the MVB pathway defect caused by loss of Doa4 function. A hallmark phenotype caused by deletion of the *DOA4* gene is the selective block in sorting of Ub-dependent MVB cargoes such as CPS, whereas sorting of Ub-independent cargoes such as Sna3 is unaffected (Reggiori and Pelham, 2001). In contrast, deletion of any class E *VPS* gene, including *BRO1*,

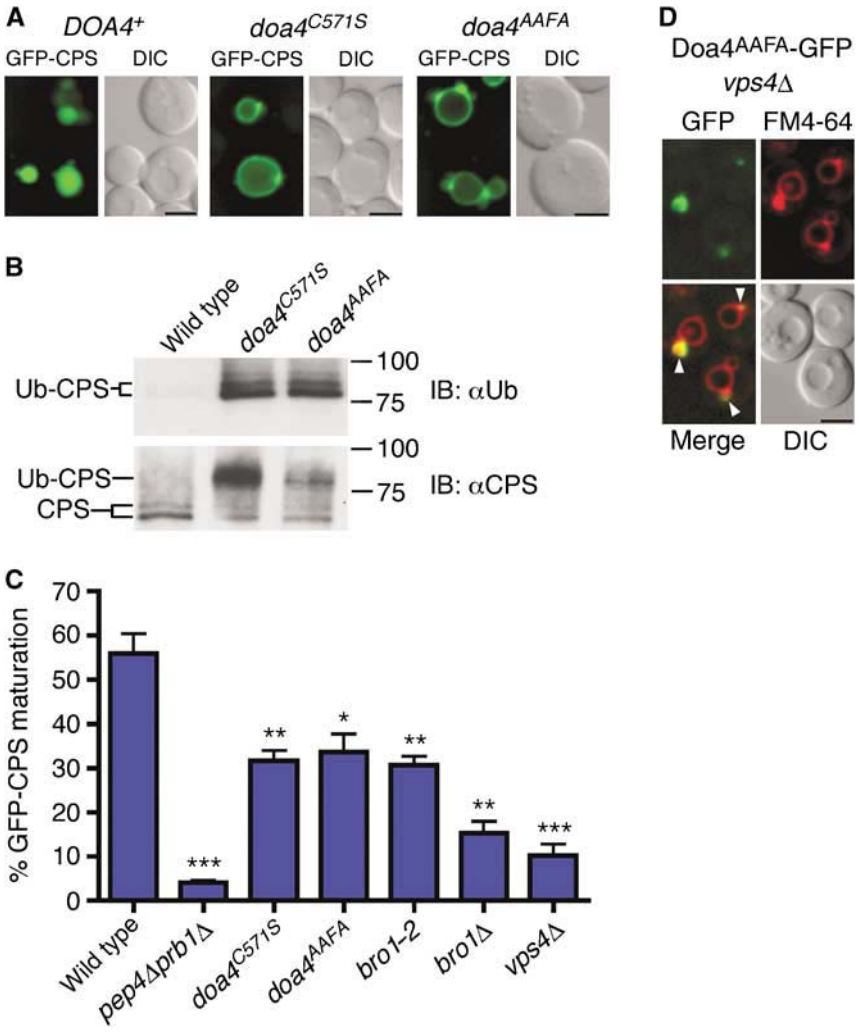

Figure 3 The Doa4 YPxL motif is necessary for cargo sorting and deubiquitination. (**A**) Fluorescence and DIC microscopy of GFP-CPS. (**B**) Denatured anti-CPS immunoprecipitations followed by anti-Ub and anti-CPS immunoblotting. Doublet bands represent differentially glycosylated forms of CPS. The slower migrating bands in the anti-Ub panel might represent more extensive Ub modification of CPS. (**C**) Quantification of GFP-CPS cleavage measured after anti-GFP immunoprecipitation from ^{35}S-labeled cell extracts; *P*-values <0.05 (*), 0.01 (**), or 0.001 (***). (**D**) Fluorescence and DIC microscopy of *vps4*Δ cells expressing the Doa4^{AAFA}-GFP fusion from a low-copy number plasmid under the control of the *DOA4* promoter. Closed arrowheads indicate class E compartments that colocalize with GFP. Scale bar, 2.5 μm (A, D).

blocks sorting of both Ub-dependent and -independent cargoes via the MVB pathway (Figure 5A) (Reggiori and Pelham, 2001). Although the general mechanism by which Bro1 function is required for sorting MVB cargoes is unknown, we reasoned that its interaction with Doa4 constitutes a subdivision of function specifically required for sorting Ub-dependent MVB cargoes. Thus, a mutation in Bro1 that prevents it from binding the YPxL motif of Doa4 but otherwise has no adverse effect on Bro1 function should block the sorting of CPS but not Sna3. Indeed, the *bro1-2* allele, which contains a premature stop codon in place of codon 820 (Figure 4A), caused mislocalization of GFP-CPS to the vacuole membrane, but did not block sorting of Sna3-GFP into the vacuole lumen (Figure 5A). Furthermore, *bro1-2* impaired GFP-CPS cleavage to a similar extent as observed in *doa4*^{AAFA} cells (Figure 3C and Supplementary Figure S2). Yeast two-hybrid analysis confirmed that the mutant Bro1-2 protein was unable to bind the Doa4 catalytic domain (Figure 4B), and fluorescence microscopy indicated that the *bro1-2* mutation had no effect on the ability of Bro1 to recruit Doa4 to endosomes (Figure 5B). Together, these observations suggested that truncation of the Bro1 C terminus prevents it from binding the YPxL motif of Doa4.

The Doa4-specific MVB sorting defect caused by the *bro1-2* mutation was further supported by three-dimensional electron tomographic modeling. In wild-type yeast cells, MVBs are spherical structures that have numerous lumenal vesicles (Figure 5C and Supplementary Video S5). In contrast, deletion of the *BRO1* gene dramatically alters the morphology of endosomes such that they consist of flattened cisternae-like structures within which lumenal vesicles are entirely absent (Figure 5D and Supplementary Video S6). This abnormal endosomal morphology is a unique characteristic caused by deletion of any class E *VPS* gene. Therefore, these aberrant structures are referred to as 'class E compartments' (Raymond *et al*, 1992; Rieder *et al*, 1996; Babst *et al*, 1997; Odorizzi *et al*, 1998). Unlike *bro1*Δ cells, *bro1-2* cells do not have class E compartments, but instead have spherical multivesicular endosomes (Figure 5E and Supplementary Video

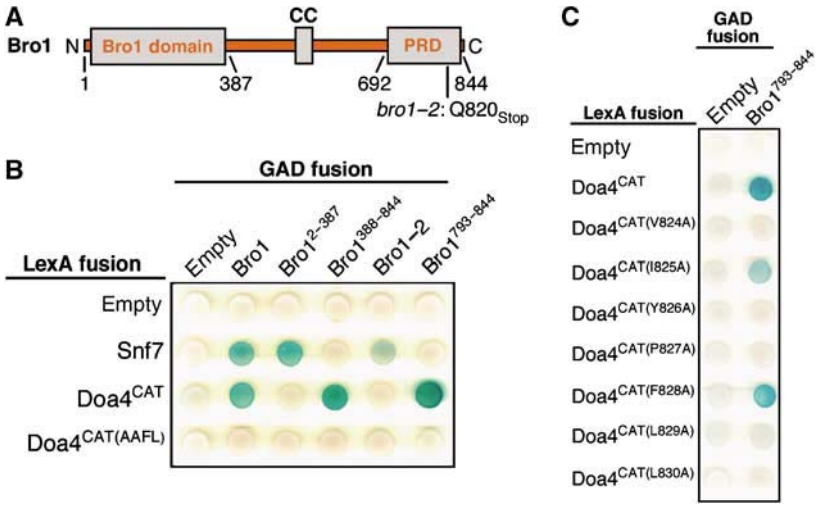

Figure 4 Bro1 interacts with the Doa4 YPxL motif. (**A**) Schematic diagram of Bro1 indicating the 'Bro1 domain', coiled-coil (CC), and proline-rich domain (PRD). The *bro1-2* mutation replaces the glutamine at position 820 with a termination codon. (**B, C**) Yeast two-hybrid analysis of the interaction between Doa4 and Bro1. Bro1 fragments fused to the Gal4 activation domain are indicated with GAD-Bro1, including the appropriate amino-acid residues. The LexA DNA-binding domain was fused to Snf7 from *A. nidulans*, $Doa4^{CAT}$, and the indicated amino-acid substitutions within $Doa4^{CAT}$.

S7), similar to those observed in $doa4^{C571S}$ cells (Figure 5F and Supplementary Video S8).

The presence of lumenal MVB vesicles in *bro1-2* and $doa4^{C571S}$ cells is consistent with both strains having a functional MVB pathway capable of sorting Sna3-GFP but not Ub-dependent cargoes such as GFP-CPS. However, closer examination revealed another phenotype caused by the *bro1-2* and $doa4^{C571S}$ mutations. The lumenal MVB vesicles of both mutant strains were predominantly smaller than MVB vesicles in wild-type cells (Figure 5G) even though the size of MVBs was unchanged (Supplementary Figure S4B). Although the molecular basis for larger lumenal MVB vesicles being absent in *bro1-2* and $doa4^{C571S}$ cells is not clear, this observation provided further evidence that truncation of Bro1 mimics the MVB pathway defects caused by loss of Doa4 function.

Overexpression of Ub restored the formation of larger lumenal vesicles in cells lacking Doa4 activity (Supplementary Figure S3C), but also caused distortions of the limiting endosomal membrane (Supplementary Figure S3D), resulting in structures we recently characterized as vesicular tubular endosomes (VTEs) (Nickerson *et al*, 2006). VTEs exist in cells lacking expression of Did2, an adaptor protein that couples Vps4 activity to ESCRT-III dissociation from endosomes. For unknown reasons, the lumenal vesicles of VTEs in *did2*Δ cells are unusually large (Nickerson *et al*, 2006). Thus, it is unclear whether the increased lumenal vesicle size caused by overexpression of Ub in cells lacking Doa4 function is simply due to replenished pools of free cellular Ub or, instead, a manifestation of the VTE morphology.

A conserved C-terminal motif in Bro1 is required for its interaction with the catalytic domain of Doa4

Based on the inability of the Bro1-2 protein to bind the Doa4 catalytic domain, we hypothesized that a C-terminal fragment of Bro1 would be sufficient for this interaction to occur. Indeed, the last 52 amino acids of Bro1 (residues 793–844) interacted with $Doa4^{CAT}$ (Figure 4B). The amino-acid sequence at the C-terminal tip of Bro1 is highly conserved among its candidate orthologs in other fungal species (Figure 6A). Therefore, we tested whether mutation of its C-terminal residues affected binding of $Bro1^{793–844}$ to $Doa4^{CAT}$. As shown in Figure 6B, this interaction was disrupted upon substitution of four alanine residues in place of the PSVF sequence spanning amino acids 831–834 of Bro1 ($Bro1^{793–844(PSVF–AAAA)}$), or upon individual substitution of alanine for P_{831}, S_{832}, V_{833}, or F_{834}. Binding also did not occur upon mutation of R_{830}, M_{838}, Y_{839}, or Y_{842}, whereas the interaction was unaffected by substitution of alanine in place of D_{835}, E_{836}, N_{837}, S_{840}, K_{841}, S_{843}, or S_{844} (Figure 6A and data not shown). Consistent with this region of Bro1 binding to the YPxL motif in Doa4, cells expressing the $bro1^{PSVF–AAAA}$ allele were defective in deubiquitination and sorting of CPS (Figure 6C and D) and contained a predominance of small lumenal MVB vesicles (Supplementary Figure S4A and Supplementary Video S9). Thus, binding of the YPxL motif in Doa4 by the conserved C terminus of Bro1 is required for Doa4-mediated deubiquitination of MVB cargoes.

Bro1 stimulates deubiquitination by Doa4

To test directly the effect of Bro1 on deubiquitination, we isolated recombinant $Doa4^{CAT}$ from bacteria and analyzed its enzymatic activity *in vitro* in the presence or absence of recombinant $Bro1^{388–844}$. Incubation of GST-$Doa4^{CAT}$ with Ub fused to 7-amino-4-methylcoumarin (Ub-AMC) resulted in a low rate of hydrolysis, as measured by emission of AMC fluorescence (Figure 7A). Addition of His_6-$Bro1^{388–844}$ to the reaction dramatically enhanced the rate of hydrolysis, but this stimulatory effect was lost when the PSVF sequence in Bro1 was mutated (Figure 7A), confirming that this motif is essential for binding to the Doa4 catalytic domain and stimulation of deubiquitination. Maximal stimulation of Ub-AMC hydrolysis was reached when His_6-$Bro1^{388–844}$ was present at 1- to 2-fold amounts relative to GST-$Doa4^{CAT}$ (Figure 7B), indicating a stoichiometric relationship.

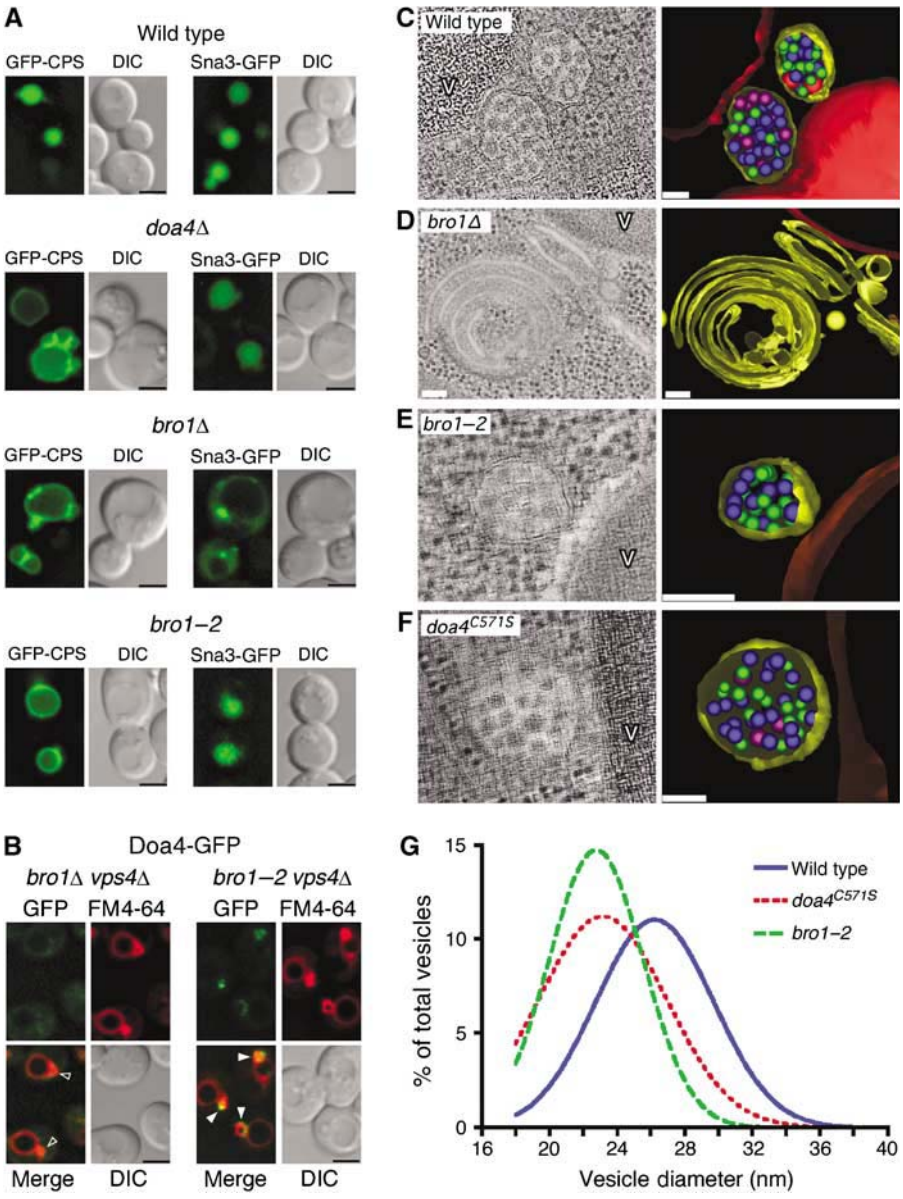

Figure 5 The C terminus of Bro1 is specifically required for Ub-dependent cargo sorting. (**A**) Fluorescence and DIC microscopy of GFP-CPS and Sna3-GFP. (**B**) Fluorescence and DIC microscopy of Doa4-GFP. Arrowheads indicate E compartments that do (closed arrowheads) or do not (open arrowheads) colocalize with GFP. Scale bar, 2.5 μm (A, B). (**C–F**) EM showing MVBs in wild-type, *bro1-2*, and *doa4*^{C571S} cells, and the class E compartment in *bro1*Δ cells. Vesicles in tomographic models have diameters indicated by green (18–23 nm), purple (24–29 nm), pink (30–35 nm), red (36–47 nm). V = vacuole. Scale bar, 0.1 μm (**G**) Distribution of MVB vesicle diameters from wild-type ($n = 330$), *bro1-2* ($n = 265$), and *doa4*^{C571S} cells ($n = 371$). Mean vesicle diameters of *bro1-2* and *doa4*^{C571S} cells differ significantly from that of wild-type cells ($P < 0.0001$).

To determine whether Bro1$^{388–844}$ increases the catalytic activity and/or substrate affinity of Doa4, we generated Michaelis–Menten curves by testing the reaction velocity at varying Ub-AMC concentrations. As shown in Figure 7C, GST-Doa4^{CAT} incubated with His$_6$-Bro1$^{388–844}$ yielded a V_{max} of Ub-AMC hydrolysis at 75.16 nmole/min, resulting in a K_M of 0.56 μM. However, the reaction velocity for GST-Doa4^{CAT} alone was linearly related to substrate concentration (Figure 7C), which precluded determination of the V_{max} and K_M. Nevertheless, we infer from Figure 7C that the K_M of Ub-AMC hydrolysis by GST-Doa4^{CAT} alone is significantly higher than the K_M of GST-Doa4^{CAT} in the presence of His$_6$-Bro1$^{388–844}$, suggesting that Bro1 increases the affinity of Doa4 for its substrate.

Discussion

Bimodal regulation of localization and activation is emerging as a paradigm for controlling the specificity of enzymes that function in multiple cellular processes (Bhattacharyya *et al*, 2006; Chen and Kass, 2006; Dard and Peter, 2006). Doa4 is a UBP in *S. cerevisiae* that removes Ub from membrane proteins targeted into the MVB pathway (Dupre and Haguenauer-Tsapis, 2001; Katzmann *et al*, 2001; Losko *et al*, 2001), and from soluble proteins targeted to proteasomes (Papa *et al*, 1999). In addition, Doa4 activity has been implicated in the coordination of DNA replication (Singer *et al*, 1996) and the DNA damage response (Fiorani *et al*, 2004). Our results indicate that Bro1 both recruits Doa4 to

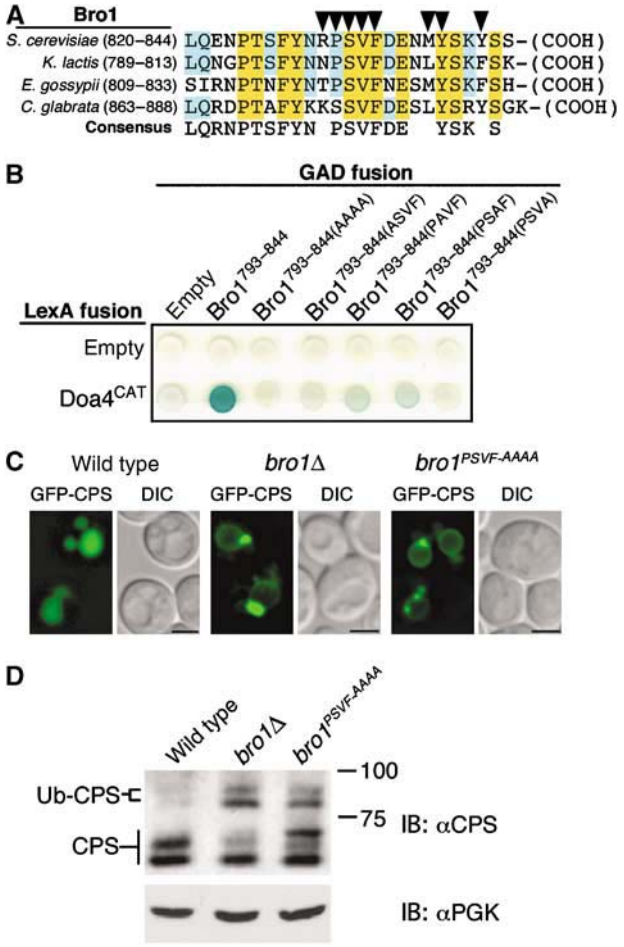

Figure 6 The Bro1 PSVF motif interacts with the Doa4 YPxL motif. (**A**) Multiple sequence alignment of the C termini of Bro1 homologs from several fungal species. Arrowheads indicate Bro1 residues required for interaction with $Doa4^{CAT}$ by two hybrid. (**B**) Yeast two-hybrid analysis of the interaction between Doa4 and Bro1. (**C**) Fluorescence and DIC microscopy of GFP-CPS. Scale bar, 2.5 μm. (**D**) Anti-CPS immunoblot of whole-cell lysates. The ~9 kDa shift in CPS corresponds to its monoubiquitinated form.

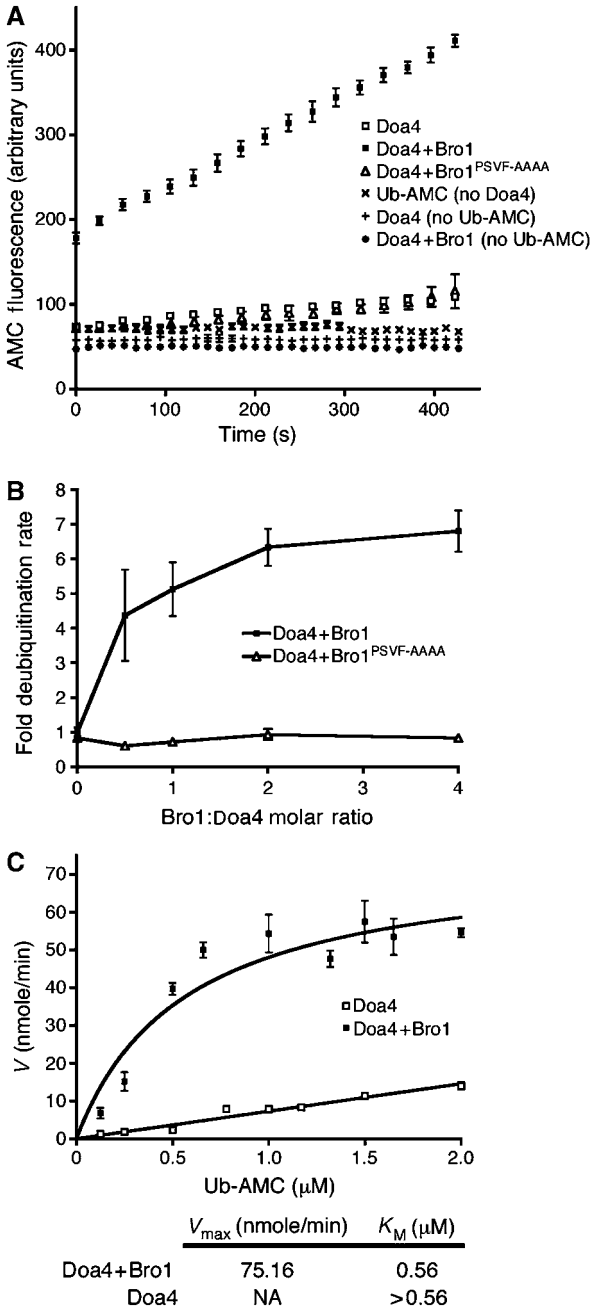

Figure 7 Bro1 stimulates Doa4-mediated deubiquitination *in vitro*. (**A**) Measurement of fluorescence generated by deubiquitination of Ub-AMC (0.4 μM; λ_{ex}: 380 nM, λ_{em}: 440 nM) using 50 nM GST-$Doa4^{406–926}$ with or without 100 nM His_6-$Bro1^{388–844}$ or His_6-$Bro1^{388–844(PSVF–AAAA)}$. All Bro1 and Doa4 proteins were purified from *E. coli* and reactions were run for 7 min in triplicate. Measurements were also taken in the absence of either enzyme or substrate to control for aberrant deubiquitination or fluorescence, respectively. (**B**) Doa4-mediated Ub-AMC hydrolysis under varying concentrations of His_6-$Bro1^{388–844}$ or His_6-$Bro1^{388–844(PSVF–AAAA)}$. GST-$Doa4^{406–926}$ and Ub-AMC concentrations were kept constant at 50 nM and 0.4 μM, respectively. The deubiquitination rate was normalized to that of GST-$Doa4^{406–926}$ in the absence of His_6-$Bro1^{388–844}$. (**C**) Ub-AMC hydrolysis by GST-$Doa4^{406–926}$ (50 nM) under varying substrate concentrations, with or without His_6-$Bro1^{388–844}$ (100 nM). All data points are represented by mean ± s.e.m.

late endosomes and stimulates its catalytic activity, thereby exerting dual modes of regulation to control the specificity of Doa4 function in the MVB pathway. Site-specific activation by Bro1 ensures that Doa4 is active during its transient association with endosomes and implies that the location and timing of Doa4 activity outside of the MVB pathway is also regulated to prevent nonspecific protein deubiquitination. Dual-regulatory mechanisms may similarly function in other cases of UBP-mediated deubiquitination. The catalytic activity of Ubp6 is stimulated by its recruitment to proteasomes (Leggett *et al*, 2002), as is the activity of Ubp8 upon its assembly into the SAGA histone acetyltransferase complex (Lee *et al*, 2005). In addition, the catalytic activity of AMSH, which belongs to the JAMM metalloprotease family of DUBs, is stimulated upon binding to the endosomal sorting factor STAM (McCullough *et al*, 2006).

The finding that Bro1 reduces the K_M of deubiquitination is consistent with a model in which it enhances substrate binding by Doa4, although the mechanism by which this occurs is unknown. In mammalian cells, Adrm1 reduces the K_M of Uch37-mediated deubiquitination by binding its non-catalytic autoinhibitory C terminus (Yao *et al*, 2006). Although Uch37 belongs to the Ub C-terminal hydrolase (UCH) family of DUBs, structural analyses indicate that the

catalytic cores of UCH and UBP enzymes are very similar (Johnston *et al*, 1999; Hu *et al*, 2002). The ability of Adrm1 to relieve autoinhibition by binding the non-catalytic C-terminal region of Uch37, however, is distinct from the mechanism by which Bro1 binds directly to the catalytic domain of Doa4 to stimulate its activity. Recent structural analysis of UBPY, the mammalian UBP most closely related to Doa4, has revealed it to be autoinhibited by β-strands and loop segments in its catalytic domain that block access to the Ub-binding site, and only after these elements are displaced, is UBPY capable of substrate binding and deubiquitination (Avvakumov *et al*, 2006). Movement of these features in UBPY was proposed to be under the control of helix 12, which might act as a hinge. Alignment of the UBPY and Doa4 catalytic domain sequences positions the YPxL motif of Doa4 adjacent to helix 12 of UBPY (Avvakumov *et al*, 2006), raising the possibility that binding of Bro1 to this site induces a structural rearrangement that provides the catalytic site of Doa4 access to ubiquitinated MVB cargoes. However, this interaction is likely to be transient, as we cannot detect stable binding between GST-Doa4^{CAT} and His$_6$-Bro1$^{388–844}$ *in vitro* (C Richter and G Odorizzi, unpublished observations).

The role of the N terminus of Doa4 in its endosomal recruitment is consistent with a modular principle of UBPs in which their non-catalytic domains mediate localization to specific subcellular sites of function (Leggett *et al*, 2002; Hu *et al*, 2005). Recent work identified four conserved amino-acid motifs in the N-terminal region of Doa4 that are required for its localization to endosomes (Amerik *et al*, 2006). However, based on analysis of an overexpressed Doa4-GFP fusion protein, the same study concluded that Bro1 is dispensable for endosomal localization of Doa4 (Amerik *et al*, 2006). Although Bro1 physically associates with the N-terminal endosomal localization region of Doa4 in cell lysates (this study) and is required for the endosomal localization of Doa4-GFP expressed at physiologically normal levels (this study and Luhtala and Odorizzi, 2004), we have also found that, when overexpressed, Doa4-GFP localizes to endosomes in the absence of Bro1 (C Richter and G Odorizzi, unpublished observations). It is likely, therefore, that another component on endosomal membranes binds Doa4, but this factor, alone, is insufficient to effectively concentrate Doa4 at endosomes under the normal conditions of low Doa4 expression. Such a factor may also stabilize the interaction between Bro1 and the Doa4 N terminus because their binding is undetectable in the yeast two-hybrid assay (C Richter and G Odorizzi, unpublished observations).

In addition to causing MVB sorting defects, loss of Doa4 function renders cells hypersensitive to canavanine, a cytotoxic arginine analog (Papa and Hochstrasser, 1993). The canavanine hypersensitivity can be rescued by fusion of the N terminus of Doa4 to the catalytic domain of its most closely related yeast homolog, Ubp5 (Amerik *et al*, 2006). However, we found that MVB cargo deubiquitination and sorting could not be rescued by an identical Doa4-Ubp5 fusion protein (nor could GFP-CPS cleavage; C Richter and G Odorizzi, unpublished observation), indicating that canavanine sensitivity is caused by a defect in Doa4 function unrelated to the MVB pathway. The inability of the Ubp5 catalytic domain to substitute for that of Doa4 led us to speculate that an endosome-associated factor might function specifically to stimulate Doa4 activity. Our discovery that Bro1 functions in this manner by binding the YPxL motif of Doa4 was guided by previous work showing that the mammalian ortholog of Bro1, Alix, binds a YPxL consensus sequence in Gag protein subunits encoded by HIV-1, EIAV, and MuLV. As a consequence, Alix is recruited to the site of viral assembly to facilitate budding of infectious virions from host cells (Puffer *et al*, 1997; Martin-Serrano *et al*, 2003; Strack *et al*, 2003; Segura-Morales *et al*, 2005). Like MVB cargoes, viral Gag proteins are ubiquitinated, but it is unclear whether Ub modification is relevant to viral budding (Morita and Sundquist, 2004). However, it is noteworthy that transplantation of the YPxL motif into recombinant viral constructs reduces the amount of Ub-conjugated Gag (Martin-Serrano *et al*, 2004), suggesting that Alix subsequently results in recruitment of a DUB in a way similar to recruitment of Doa4 by Bro1.

YPxL motifs also mediate protein interactions with homologs of Bro1 that have no functional connection to the MVB pathway. Rim101 in *S. cerevisiae* and PacC in *Aspergillus nidulans* are YPxL-containing transcription factors that undergo proteolytic cleavage and activation upon interacting with the Bro1 homologs Rim20 and PalA, respectively (Xu and Mitchell, 2001; Vincent *et al*, 2003). Although the C-terminal PSVF-containing sequence in Bro1 is conserved among the predicted functional orthologs of Bro1 in fungal species, it is not found in Rim20 and PalA. Similarly, the C termini of Bro1 and Alix share little sequence homology, and the region of Alix that binds viral YPxL sequences is located in the middle of the protein between its Bro1 domain and proline-rich region (Fisher *et al*, 2007; Lee *et al*, 2007). Therefore, any similarity between the PSVF motif of Bro1 and the YPxL-binding regions of Alix, Rim20, and PalA might only be apparent at the level of tertiary structure.

Mutations that disrupt the PSVF motif in Bro1 phenocopy the loss of Doa4 function by blocking the sorting of CPS, a Ub-dependent MVB cargo, whereas the sorting of Sna3, a Ub-independent cargo, continues normally. Accordingly, *bro1-2* and *bro1$^{PSVF–AAAA}$* mutant cells both resemble *doa4^{C571S}* cells in that they have MVBs rather than the class E compartments that are characteristically observed upon deletion of *BRO1* or any other class E *VPS* gene (Raymond *et al*, 1992; Rieder *et al*, 1996; Babst *et al*, 1997; Odorizzi *et al*, 1998). Defining how class E Vps proteins coordinate both MVB cargo sorting and lumenal vesicle formation is a major challenge in understanding the molecular mechanism of MVB function. Our results clearly indicate that a division of labor exists for Bro1 in these processes. Insight into the specific role that Bro1 has in forming lumenal MVB vesicles might be gleaned from studies indicating that its mammalian ortholog, Alix, binds lysobisphospatidic acid (LBPA) to regulate the dynamic ability of this lipid to promote either fission or fusion of lumenal MVB membranes (Matsuo *et al*, 2004; Le Blanc *et al*, 2005). However, a similar role for Bro1 in regulating membrane dynamics likely differs mechanistically because LBPA has not been detected in yeast.

The range of MVB vesicle diameters observed in wild-type yeast cells sharply contrasts with the predominantly small vesicles observed in cells lacking Doa4 activity. How lumenal MVB vesicle size correlates with Doa4 function is unknown. If deubiquitination has a direct role in MVB vesicle size determination, it might be coupled to activation of a molecular machinery that controls the formation of larger vesicles

within which Ub-dependent cargoes such as CPS are selectively packaged, while a separate machinery might operate independently to form smaller vesicles that transport Ub-independent cargoes such as Sna3. Alternatively, lumenal MVB vesicle size might be determined by the influx of cargoes into the pathway. Most yeast cargoes are dependent upon the cycle of ubiquitination and deubiquitination and, as such, are blocked from entering the MVB pathway in cells lacking Doa4 activity (Loayza and Michaelis, 1998; Dupre and Haguenauer-Tsapis, 2001; Reggiori and Pelham, 2001; Urbanowski and Piper, 2001). Deubiquitination might, therefore, have no direct influence on MVB vesicle formation, with smaller vesicles providing adequate surface area to accommodate a decreased cargo load in the absence of Doa4 function.

Materials and methods

Yeast strains and plasmid construction

For information, see Supplementary data.

Fluorescence microscopy

Strains were grown to logarithmic phase at 30°C in synthetic medium before observation at room temperature using a Zeiss Axioplan 2 microscope with an NA 1.40 oil-immersion objective (Carl Zeiss MicroImaging Inc.). Fluorescence and differential interference contrast (DIC) images were acquired with a Cooke Sensicam digital camera (Applied Scientific Instruments Inc.) and processed using Slidebook (Intelligent Imaging Innovations) and Photoshop 7.0 software (Adobe). Cells were stained with FM4-64 (Molecular Probes Inc.) using a pulse–chase procedure as described previously (Odorizzi *et al*, 2003).

High-pressure freeze substitution and electron tomography

Cells were high-pressure frozen, freeze-substituted with 0.1% uranyl acetate, 0.25% glutaraldehyde, anhydrous acetone at −90°C, embedded in Lowicryl HM20, and polymerized under UV at −50°C (Winey *et al*, 1995). Semi-thick sections (200 nm) were placed on rhodium-plated formvar-coated copper slot grids and mapped on a Phillips CM10 TEM at 80 kV. Dual tilt series images were collected from +60° to −60° with 1° increments at 200 kV using a Tecnai 20 FEG (FEI). Tomograms were imaged at ×29 000 with a 0.77 nm pixel (binning 2). Sections were coated on both sides with 15-nm fiducial gold for reconstruction of back projections using IMOD software (Kremer *et al*, 1996). 3dmod software was used for mapping structure surface areas. Mean *z*-scale values for sections were within 3%. Best-fit sphere models were used to measure vesicle diameters to the outer leaflet of membrane bilayers. IMOD calculated limiting membrane surface areas using three-dimensional mesh structures derived from closed contours drawn each 3.85 nm using imodmesh. For quantitation, vesicles from 12–13 random MVBs were measured from 4–5 cells of each strain and analyzed using the Gaussian curve fit of the Prism software (GraphPad Software).

Immunoprecipitation and Western blotting

Denatured immunoprecipitations to detect Ub-CPS were performed as described previously (Katzmann *et al*, 2001; Luhtala and Odorizzi, 2004). The 0.5 A_{600} equivalents were resolved by SDS–PAGE, transferred to nitrocellulose, and analyzed by Western blot using rabbit anti-CPS polyclonal antiserum (Cowles *et al*, 1997), anti-Ub monoclonal antibodies (Zymed), and anti-phosphoglycerate kinase (PGK) monoclonal antibodies (Invitrogen). For native immunoprecipitations of Doa4$^{1-560}$-TEV-HA, yeast lysates prepared as previously described (Luhtala and Odorizzi, 2004) were incubated with mouse anti-HA monoclonal antibodies (Covance) and protein G–Sepharose beads (GE Healthcare) for 2 h at 4°C, after which the beads were collected by centrifugation and washed (Luhtala and Odorizzi, 2004), and 10 A_{600} equivalents of immunoprecipitates or 0.5 A_{600} equivalents of total lysate were resolved by SDS–PAGE, transferred to nitrocellulose, and analyzed by Western blot using rabbit anti-Bro1 polyclonal antiserum (Odorizzi *et al*, 2003) and mouse anti-HA monoclonal antibodies (Covance). For pulse–chase metabolic labeling, 5 A_{600} equivalents of yeast cells were incubated with 100 μCi ^{35}S-labeled methionine/cysteine for 10 min at 30°C, followed by the addition of chase mixture (5 mM methionine, 1 mM cysteine, and 0.2% yeast extract) for 0 or 30 min. Afterward, cells were precipitated by the addition of 10% (vol/vol) trichloroacetic acid, cell lysates were prepared under denaturing conditions, and immunoprecipitations of GFP-CPS were performed as previously described (Katzmann *et al*, 2001; Luhtala and Odorizzi, 2004) using anti-GFP polyclonal antiserum (Odorizzi *et al*, 1998). Immunoprecipitates were resolved by SDS–PAGE and exposed to a storage phosphor screen (GE Healthcare), and then developed by a Storm® Phosphorimager (GE Healthcare) and quantified using ImageQuant™ TL (GE Healthcare). All samples were tested in triplicate and the Prism software (Graphpad Software) was used for statistical analysis.

Isolation of the bro1-2 allele

BRO1 was PCR-amplified using Taq polymerase (Invitrogen) under error-prone conditions (Guthrie and Fink, 2002) to generate a library of random mutant *bro1* alleles that were pooled and cotransformed into yeast strain KGY1 (Luhtala and Odorizzi, 2004) together with pGO221 (pRS416 containing the *BRO1* gene) that had been linearized by *Eco*RI/*Hin*dIII digestion. *In vivo* homologous recombination yielded >10 000 colonies of KGY1, each of which contained one repaired plasmid encoding a single *bro1* allele. KGY1 expresses the carboxypeptidase Y-invertase reporter fusion protein, which is secreted upon loss of Bro1 function (Luhtala and Odorizzi, 2004). Thus, colonies of KGY1 transformed with plasmids encoding non-functional mutant *bro1* alleles were identified based on the detection of secreted invertase activity using a colorimetric agar overlay assay (Darsow *et al*, 2000; Luhtala and Odorizzi, 2004). Whole-cell lysates prepared from clones secreting invertase were analyzed by SDS–PAGE and Western blotting using rabbit anti-Bro1 antiserum to eliminate plasmids not expressing Bro1. The remaining plasmids were isolated from yeast and subjected to DNA sequence analysis. Among the mutant *bro1* alleles isolated by this procedure, the *bro1-2* allele was the only one that was capable of sorting Sna3-GFP but not GFP-CPS via the MVB pathway.

Yeast two-hybrid

CTY10.5d was transformed with *GAD* and *LEXA* fusions (Vincent *et al*, 2003), patched onto agar medium, allowed to grow for 3 days, then lysed by exposure to chloroform vapor for 30 min before overlay with 0.6% agar containing Z-buffer (60 mM Na_2HPO_4, 40 mM $NaH_2PO_4 \cdot H_20$, 10 mM KCl, 1 mM $MgSO_4 \cdot 7H_20$, 0.2% β-mercaptoethanol, and 0.67 mg/ml X-gal). Blue/white analysis was performed after 6 h to identify interactions.

In vitro deubiquitination assays

GST-Doa4$^{406-926}$, His$_6$-Bro1$^{388-844}$, and His$_6$-Bro1$^{388-844(PSVF-AAAA)}$ were expressed in *Escherichia coli* BL21-CodonPlus (DE3) cells (Stratagene) by induction with 0.5 mM isopropyl-β-D-thiogalactoside at 20°C for 18 h and purified using glutathione–Sepharose (GE Healthcare) or TALON metal affinity resin (Clontech). For deubiquitination reactions, 50 nM GST-Doa4$^{406-926}$ was incubated with or without His$_6$-Bro1$^{388-844}$, or His$_6$-Bro1$^{388-844(PSVF-AAAA)}$, in reaction buffer (50 mM HEPES pH 7.5, 2 mM DTT, and 0.1 mg/ml BSA) for 30 min at 25°C in 96-well plates. Reactions were initiated by the addition of Ub-AMC (Boston Biochem) and analyzed by a Tecan Safire II fluorescence plate reader (λ_{ex}: 380 nM, λ_{em}: 440 nM), which maintained the reaction at 25°C. All samples were tested in triplicate and Prism (GraphPad Software) was used for statistical analysis and nonlinear fit to Michaelis–Menten kinetics.

Supplementary data

Supplementary data are available at *The EMBO Journal* Online (http://www.embojournal.org).

Acknowledgements

We thank Sarah Altschuler and Megan Wemmer (University of Colorado) for plasmid and yeast strain construction, Doug Burch (University of Colorado) for yeast strain construction and electron microscopy, Amy Palmer (University of Colorado) for the use of the

Tecan Safire II fluorescence plate reader, Olivier Vincent (Centro de Investigaciones Biológicas del CSIC) for providing the yeast two-hybrid strain and plasmids, Mark Hochstrasser (Yale University) for providing plasmids encoding Ub and the $Doa4^{N}$-$Ubp5^{CAT}$ fusion, and Eric Cooper (Johns Hopkins University) for advice on DUB kinetic analysis. This work was supported by NIH training grant GM08759 (CR) and NIH RO1 GM065505 (GO). GO is an Arnold and Mabel Beckman Foundation Young Investigator.

References

Amerik A, Sindhi N, Hochstrasser M (2006) A conserved late endosome-targeting signal required for Doa4 deubiquitylating enzyme function. *J Cell Biol* **175:** 825–835

Amerik AY, Hochstrasser M (2004) Mechanism and function of deubiquitinating enzymes. *Biochim Biophys Acta* **1695:** 189–207

Avvakumov GV, Walker JR, Xue S, Finerty Jr PJ, Mackenzie F, Newman EM, Dhe-Paganon S (2006) Amino-terminal dimerization, NRDP1 (FLRF)–rhodanese interaction, and inhibited catalytic domain conformation of the ubiquitin specific protease 8 (USP8/UBPY). *J Biol Chem* **281:** 38061–38070

Babst M, Katzmann DJ, Estepa-Sabal EJ, Meerloo T, Emr SD (2002) Escrt-III: an endosome-associated heterooligomeric protein complex required for mvb sorting. *Dev Cell* **3:** 271–282

Babst M, Sato TK, Banta LM, Emr SD (1997) Endosomal transport function in yeast requires a novel AAA-type ATPase, Vps4p. *EMBO J* **16:** 1820–1831

Bhattacharyya RP, Remenyi A, Good MC, Bashor CJ, Falick AM, Lim WA (2006) The Ste5 scaffold allosterically modulates signaling output of the yeast mating pathway. *Science* **311:** 822–826

Chen L, Kass RS (2006) Dual roles of the A kinase-anchoring protein Yotiao in the modulation of a cardiac potassium channel: a passive adaptor versus an active regulator. *Eur J Cell Biol* **85:** 623–626

Clague MJ, Urbe S (2006) Endocytosis: the DUB version. *Trends Cell Biol* **16:** 551–559

Cowles CR, Snyder WB, Burd CG, Emr SD (1997) Novel Golgi to vacuole delivery pathway in yeast: identification of a sorting determinant and required transport component. *EMBO J* **16:** 2769–2782

Dard N, Peter M (2006) Scaffold proteins in MAP kinase signaling: more than simple passive activating platforms. *Bioessays* **28:** 146–156

Darsow T, Odorizzi G, Emr SD (2000) Invertase fusion proteins for analysis of protein trafficking in yeast. *Methods Enzymol* **327:** 95–106

Dupre S, Haguenauer-Tsapis R (2001) Deubiquitination step in the endocytic pathway of yeast plasma membrane proteins: crucial role of Doa4p ubiquitin isopeptidase. *Mol Cell Biol* **21:** 4482–4494

Fiorani P, Reid RJ, Schepis A, Jacquiau HR, Guo H, Thimmaiah P, Benedetti P, Bjornsti MA (2004) The deubiquitinating enzyme Doa4p protects cells from DNA topoisomerase I poisons. *J Biol Chem* **279:** 21271–21281

Fisher RD, Chung H, Zhai Q, Robinson H, Sundquist WI, Hill CP (2007) Structural and biochemical studies of ALIX/AIP1 and its role in retrovirus budding. *Cell* **128:** 841–852

Guthrie C, Fink GR (eds). (2002) *Guide to Yeast Genetics and Molecular Biology*. Academic Press: San Diego

Hu M, Li P, Li M, Li W, Yao T, Wu JW, Gu W, Cohen RE, Shi Y (2002) Crystal structure of a UBP-family deubiquitinating enzyme in isolation and in complex with ubiquitin aldehyde. *Cell* **111:** 1041–1054

Hu M, Li P, Song L, Jeffrey PD, Chenova TA, Wilkinson KD, Cohen RE, Shi Y (2005) Structure and mechanisms of the proteasome-associated deubiquitinating enzyme USP14. *EMBO J* **24:** 3747–3756

Hurley JH, Emr SD (2006) The ESCRT complexes: structure and mechanism of a membrane-trafficking network. *Annu Rev Biophys Biomol Struct* **35:** 277–298

Johnston SC, Riddle SM, Cohen RE, Hill CP (1999) Structural basis for the specificity of ubiquitin C-terminal hydrolases. *EMBO J* **18:** 3877–3887

Katzmann DJ, Babst M, Emr SD (2001) Ubiquitin-dependent sorting into the multivesicular body pathway requires the function of a conserved endosomal protein sorting complex, ESCRT-I. *Cell* **106:** 145–155

Kim J, Sitaraman S, Hierro A, Beach BM, Odorizzi G, Hurley JH (2005) Structural basis for endosomal targeting by the Bro1 domain. *Dev Cell* **8:** 937–947

Kim JH, Park KC, Chung SS, Bang O, Chung CH (2003) Deubiquitinating enzymes as cellular regulators. *J Biochem (Tokyo)* **134:** 9–18

Kremer JR, Mastronarde DN, McIntosh JR (1996) Computer visualization of three-dimensional image data using IMOD. *J Struct Biol* **116:** 71–76

Le Blanc I, Luyet PP, Pons V, Ferguson C, Emans N, Petiot A, Mayran N, Demaurex N, Faure J, Sadoul R, Parton RG, Gruenberg J (2005) Endosome-to-cytosol transport of viral nucleocapsids. *Nat Cell Biol* **7:** 653–664

Lee KK, Florens L, Swanson SK, Washburn MP, Workman JL (2005) The deubiquitylation activity of Ubp8 is dependent upon Sgf11 and its association with the SAGA complex. *Mol Cell Biol* **25:** 1173–1182

Lee S, Joshi A, Nagashima K, Freed EO, Hurley JH (2007) Structural basis for viral late-domain binding to Alix. *Nat Struct Mol Biol* **14:** 194–199

Leggett DS, Hanna J, Borodovsky A, Crosas B, Schmidt M, Baker RT, Walz T, Ploegh H, Finley D (2002) Multiple associated proteins regulate proteasome structure and function. *Mol Cell* **10:** 495–507

Loayza D, Michaelis S (1998) Role for the ubiquitin-proteasome system in the vacuolar degradation of Ste6p, the a-factor transporter in *Saccharomyces cerevisiae*. *Mol Cell Biol* **18:** 779–789

Losko S, Kopp F, Kranz A, Kolling R (2001) Uptake of the ATP-binding cassette (ABC) transporter Ste6 into the yeast vacuole is blocked in the doa4 Mutant. *Mol Biol Cell* **12:** 1047–1059

Luhtala N, Odorizzi G (2004) Bro1 coordinates deubiquitination in the multivesicular body pathway by recruiting Doa4 to endosomes. *J Cell Biol* **166:** 717–729

Martin-Serrano J, Perez-Caballero D, Bieniasz PD (2004) Context-dependent effects of L domains and ubiquitination on viral budding. *J Virol* **78:** 5554–5563

Martin-Serrano J, Yarovoy A, Perez-Caballero D, Bieniasz PD (2003) Divergent retroviral late-budding domains recruit vacuolar protein sorting factors by using alternative adaptor proteins. *Proc Natl Acad Sci USA* **100:** 12414–12419

Matsuo H, Chevallier J, Mayran N, Le Blanc I, Ferguson C, Faure J, Blanc NS, Matile S, Dubochet J, Sadoul R, Parton RG, Vilbois F, Gruenberg J (2004) Role of LBPA and Alix in multivesicular liposome formation and endosome organization. *Science* **303:** 531–534

McCullough J, Row PE, Lorenzo O, Doherty M, Beynon R, Clague MJ, Urbe S (2006) Activation of the endosome-associated ubiquitin isopeptidase AMSH by STAM, a component of the multivesicular body-sorting machinery. *Curr Biol* **16:** 160–165

Mizuno E, Iura T, Mukai A, Yoshimori T, Kitamura N, Komada M (2005) Regulation of epidermal growth factor receptor down-regulation by UBPY-mediated deubiquitination at endosomes. *Mol Biol Cell* **16:** 5163–5174

Morita E, Sundquist WI (2004) Retrovirus budding. *Annu Rev Cell Dev Biol* **20:** 395–425

Nickerson DP, West M, Odorizzi G (2006) Did2 coordinates Vps4-mediated dissociation of ESCRT-III from endosomes. *J Cell Biol* **175:** 715–720

Nikko E, Andre B (2007) Evidence for a direct role of the Doa4 deubiquitinating enzyme in protein sorting into the MVB pathway. *Traffic* (in press)

Odorizzi G, Babst M, Emr SD (1998) Fab1p PtdIns(3)P 5-kinase function essential for protein sorting in the multivesicular body. *Cell* **95:** 847–858

Odorizzi G, Katzmann DJ, Babst M, Audhya A, Emr SD (2003) Bro1 is an endosome-associated protein that functions in the MVB pathway in *Saccharomyces cerevisiae*. *J Cell Sci* **116:** 1893–1903

Papa FR, Amerik AY, Hochstrasser M (1999) Interaction of the Doa4 deubiquitinating enzyme with the yeast 26S proteasome. *Mol Biol Cell* **10:** 741–756

Papa FR, Hochstrasser M (1993) The yeast DOA4 gene encodes a deubiquitinating enzyme related to a product of the human tre-2 oncogene. *Nature* **366:** 313–319

Puffer BA, Parent LJ, Wills JW, Montelaro RC (1997) Equine infectious anemia virus utilizes a YXXL motif within the late assembly domain of the Gag p9 protein. *J Virol* **71:** 6541–6546

Raymond CK, Howald-Stevenson I, Vater CA, Stevens TH (1992) Morphological classification of the yeast vacuolar protein sorting mutants: evidence for a prevacuolar compartment in class E vps mutants. *Mol Biol Cell* **3:** 1389–1402

Reggiori F, Pelham HR (2001) Sorting of proteins into multivesicular bodies: ubiquitin-dependent and -independent targeting. *EMBO J* **20:** 5176–5186

Rieder SE, Banta LM, Kohrer K, McCaffery JM, Emr SD (1996) Multilamellar endosome-like compartment accumulates in the yeast vps28 vacuolar protein sorting mutant. *Mol Biol Cell* **7:** 985–999

Row PE, Prior IA, McCullough J, Clague MJ, Urbe S (2006) The ubiquitin isopeptidase UBPY regulates endosomal ubiquitin dynamics and is essential for receptor down-regulation. *J Biol Chem* **281:** 12618–12624

Segura-Morales C, Pescia C, Chatellard-Causse C, Sadoul R, Bertrand E, Basyuk E (2005) Tsg101 and Alix interact with murine leukemia virus Gag and cooperate with Nedd4 ubiquitin ligases during budding. *J Biol Chem* **280:** 27004–27012

Singer JD, Manning BM, Formosa T (1996) Coordinating DNA replication to produce one copy of the genome requires genes that act in ubiquitin metabolism. *Mol Cell Biol* **16:** 1356–1366

Strack B, Calistri A, Craig S, Popova E, Gottlinger HG (2003) AIP1/ALIX is a binding partner for HIV-1 p6 and EIAV p9 functioning in virus budding. *Cell* **114:** 689–699

Urbanowski JL, Piper RC (2001) Ubiquitin sorts proteins into the intralumenal degradative compartment of the late-endosome/vacuole. *Traffic* **2:** 622–630

Vincent O, Rainbow L, Tilburn J, Arst Jr HN, Penalva MA (2003) YPXL/I is a protein interaction motif recognized by aspergillus PalA and its human homologue, AIP1/Alix. *Mol Cell Biol* **23:** 1647–1655

Winey M, Mamay CL, O'Toole ET, Mastronarde DN, Giddings Jr TH, McDonald KL, McIntosh JR (1995) Three-dimensional ultrastructural analysis of the *Saccharomyces cerevisiae* mitotic spindle. *J Cell Biol* **129:** 1601–1615

Xu W, Mitchell AP (2001) Yeast PalA/AIP1/Alix homolog Rim20p associates with a PEST-like region and is required for its proteolytic cleavage. *J Bacteriol* **183:** 6917–6923

Yao T, Song L, Xu W, DeMartino GN, Florens L, Swanson SK, Washburn MP, Conaway RC, Conaway JW, Cohen RE (2006) Proteasome recruitment and activation of the Uch37 deubiquitinating enzyme by Adrm1. *Nat Cell Biol* **8:** 994–1002

